# The $S_0$ State of Photosystem II Induced by Hydroxylamine: Differences between the Structure of the Manganese Complex in the $S_0$ and $S_1$ States Determined by X-ray Absorption Spectroscopy†

R. D. Guiles,‡,§ Vittal K. Yachandra,‡ Ann E. McDermott,‡,§ James L. Cole,‡,§ S. L. Dexheimer,‡,∥ R. D. Britt,‡,∥ Kenneth Sauer,‡,§ and Melvin P. Klein*,‡

*Laboratory of Chemical Biodynamics, Lawrence Berkeley Laboratory, and Departments of Chemistry and Physics, University of California, Berkeley, California 94720*

*Received December 20, 1988; Revised Manuscript Received May 26, 1989*

ABSTRACT: Hydroxylamine at low concentrations causes a two-flash delay in the first maximum flash yield of oxygen evolved from spinach photosystem II (PSII) subchloroplast membranes that have been excited by a series of saturating flashes of light. Untreated PSII membrane preparations exhibit a multiline EPR signal assigned to a manganese cluster and associated with the $S_2$ state when illuminated at 195 K, or at 273 K in the presence of 3-(3,4-dichlorophenyl)-1,1-dimethylurea (DCMU). We used the extent of suppression of the multiline EPR signal observed in samples illuminated at 195 K to determine the fraction of PSII reaction centers set back to a hydroxylamine-induced $S_0$-like state, which we designate $S_0$*. The manganese K-edge X-ray absorption edges for dark-adapted PSII preparations with or without hydroxylamine are virtually identical. This indicates that, despite its high binding affinity to the oxygen-evolving complex (OEC) in the dark, hydroxylamine does not reduce chemically the manganese cluster within the OEC in the dark. After a single turnover of PSII, a shift to lower energy is observed in the inflection of the Mn K-edge of the manganese cluster. We conclude that, in the presence of hydroxylamine, illumination causes a reduction of the OEC, resulting in a state resembling $S_0$. This lower Mn K-edge energy of $S_0$*, relative to the edge of $S_1$, implies the storage and stabilization of an oxidative equivalent within the manganese cluster during the $S_0 \rightarrow S_1$ state transition. An analysis of the extended X-ray absorption fine structure (EXAFS) of the $S_0$* state indicates that a significant structural rearrangement occurs between the $S_0$* and $S_1$ states. The X-ray absorption edge position and the structure of the manganese cluster in the $S_0$* state are indicative of a heterogeneous mixture of formal valences of manganese including one Mn(II) which is not present in the $S_1$ state.

The mechanism of photosynthetic water oxidation is a complex light-driven four-electron transfer process involving a membrane-bound chlorophyll–protein complex. The current phenomenological model of photosynthetic water oxidation involves five intermediate states, commonly designated $S_0$–$S_4$ (Kok et al., 1970). This is based on a remarkable phenomenon first observed by Joliot et al. (1969); they found that the oxygen evolved when dark-adapted chloroplasts are excited by a series of short saturating flashes of light occurs in discrete pulses which exhibit a periodicity of four in amplitude. The first maximum flash yield of oxygen was observed on the third flash and thereafter on every fourth flash. Thus, the $S_1$ state is the dominant state present in dark-adapted chloroplasts. The $S_4$ state is a transient state that decays to produce the $S_0$ state concurrent with the release of $O_2$. Absorption of a photon by the photosystem II (PSII)[1] reaction center produces a single oxidative equivalent. The coupling of four sequential photoevents to the oxidation of two water molecules in the production of a molecule of oxygen is now known to involve a cluster of manganese atoms [for a review, see Babcock (1987)]. The first spectroscopic evidence for the involvement of manganese came from the discovery of a multiline EPR signal with hyperfine structure characteristic of manganese (Dismukes & Siderer, 1981). On the basis of its flash dependence, the multiline EPR signal was associated with the $S_2$ state.

It has been suggested that the manganese cluster is the binding site of the substrate water. There is some indication of direct ligation of water to manganese from studies of line broadening of the multiline EPR signal upon $H_2{}^{17}O$ exchange (Hansson et al., 1986) and from line narrowing which occurs upon $^2H_2O$ exchange (Nugent, 1987). However, the assertion of direct binding is based principally on studies involving "water analogues" which inhibit or alter the normal cycle of oxygen evolution. Ammonia and a few low molecular weight amines competitively inhibit water oxidation (Sandusky & Yocum, 1983, 1984, 1986). Ammonia has been shown to alter the properties of the multiline EPR signal (Beck et al., 1986).

† This work was supported by a grant from the National Science Foundation (PCM 84-16676) and by the Director, Office of Energy Research, Office of Basic Energy Sciences, Division of Biological Energy Research of the U.S. Department of Energy under Contract DE-AC03-76SF00098. Synchrotron radiation facilities were provided by the Stanford Synchrotron Radiation Laboratory, which is supported by the Office of Basic Energy Sciences, U.S. Department of Energy, and by the NIH Biotechnology Program, Division of Research Resources. This is paper 11 in the series "The State of Manganese in the Photosynthetic Apparatus".

* To whom correspondence should be addressed.

‡ Laboratory of Chemical Biodynamics, Lawrence Berkeley Laboratory.

§ Department of Chemistry.

∥ Department of Physics.

[1] Abbreviations: DCMU, 3-(3,4-dichlorophenyl)-1,1-dimethylurea; EPR, electron paramagnetic resonance; EXAFS, extended X-ray absorption fine structure; MES, 4-morpholineethanesulfonic acid; MLS, multiline signal; OEC, oxygen-evolving complex; PPBQ, phenyl-*p*-benzoquinone; PSII, photosystem II; $Q_{400}$, the high-potential acceptor of PSII.

0006-2960/90/0429-486$02.50/0 

Scheme I

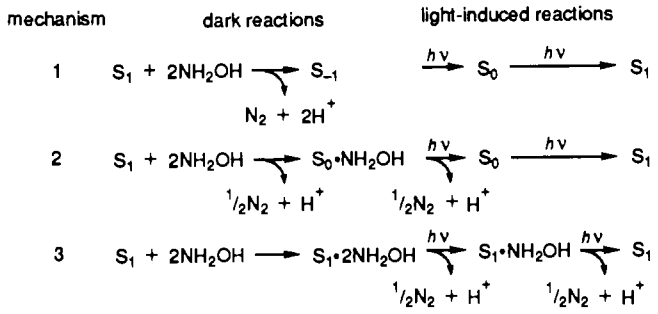


This has been taken as evidence of direct ligation of a "water analogue" to the manganese cluster.

Another class of low molecular weight "water analogues" includes hydroxylamine, hydrogen peroxide, and hydrazine. At low concentration these mild reducing agents do not inhibit steady-state oxygen evolution. However, they alter the normal light-driven cycle. Low concentrations of hydroxylamine (Bouges, 1971), hydrogen peroxide (Velthuys & Kok, 1978), and hydrazine (Kok & Velthuys, 1977) cause a two-flash delay in the occurrence of the first maximum flash yield of oxygen (i.e., the first maximum flash yield of oxygen is delayed until the fifth flash). Of these three molecules, the effect of hydroxylamine has been studied most extensively. Several mechanisms have been proposed to explain the effect of hydroxylamine. These mechanisms differ in the extent to which the oxygen-evolving complex is purportedly reduced in the dark (Bouges-Bocquet, 1973). The details of three mechanisms described below are summarized in Scheme I. In dark-adapted chloroplast suspensions incubated with low concentrations of hydroxylamine, a two-electron reduction of the oxygen-evolving complex (OEC) has been proposed to occur in the dark, resulting in a superreduced state that has been designated $S_{-1}$ (mechanism 1 in Scheme I). Alternatively, it has been suggested that a one-electron reduction occurs in the dark (generating the $S_0$ state) and that a second one-electron reduction occurs after one turnover of PSII (mechanism 2 in Scheme I). Finally, it has been suggested that two molecules of hydroxylamine bind to the OEC in the dark and that a single-electron reduction occurs during each of two successive turnovers of PSII (mechanism 3 in Scheme I). This proposed mechanism leaves the OEC poised in the $S_1$ state throughout this process.

In this report, we present the results of a Mn K-edge X-ray absorption spectroscopy study of the effect of hydroxylamine on the manganese complex in PSII. At high concentrations of hydroxylamine (e.g., 1–2 mM) the manganese in chloroplast (Cheniae & Martin, 1970) or PSII membrane preparations (Tamura & Cheniae, 1985) is irreversibly released as $Mn^{2+}$. The principal focus of this report has been to investigate the reversible effects occurring at low concentrations of hydroxylamine. We will refer to the state of the OEC generated by incubating dark-adapted PSII membrane preparations with low concentrations of hydroxylamine in the dark as $S_1 \cdot NH_2OH$ state. The state of the OEC generated by continuous illumination of $S_1 \cdot NH_2OH$ preparations at 195 K will be referred to as the $S_0$* state. X-ray absorption spectroscopy is an element-specific technique capable of yielding information directly about the oxidation state (Kirby et al., 1981a; Sauer et al., 1988) and immediate ligation sphere of the absorbing element [for a review, see Powers (1982)]. We have used this technique to address two aspects of the effect of hydroxylamine: (1) We have examined the extent of reduction of the manganese in PSII occurring in the dark upon addition of hydroxylamine. Changes in the oxidation state of manganese were also examined after continuous illumination at 195 K. (2) Extended X-ray absorption fine structure analysis provides a means of determining the number, the identity, and the distances of ligating atoms from the absorbing atom. Assuming that the hydroxylamine-induced $S_0$ ($S_0$*) state is the same as the normal $S_0$ state, an examination of differences between the structure of the hydroxylamine-induced $S_0$ state and the $S_1$ state may reflect structural rearrangements important to an understanding of the mechanism of oxygen evolution.

## Experimental Procedures

*Preparation of PSII Membranes for X-ray Absorption Measurements.* Oxygen-evolving PSII subchloroplast membranes were prepared as previously described (Yachandra et al., 1986a). Because of the instability of hydroxylamine solutions, hydroxylamine-treated samples were prepared by diluting volumes of freshly prepared 1 mM stock solutions into 20-mL volumes of PSII subchloroplast membranes suspended at 3.5 mg/mL chlorophyll. Samples containing final concentrations of 40, 60, and 100 $\mu$M hydroxylamine were prepared. Samples were allowed to stand in the dark for 30 min to ensure complete reaction. After 30 min an ethanolic solution of DCMU was added to the PSII membrane suspension to bring the final concentration of DCMU to 50 $\mu$M.

Samples for X-ray absorption spectroscopy were prepared by pelleting PSII subchloroplast membranes at 35000$g$ for 1 h. Tightly packed pellets containing ~30% glycerol were transferred to Lucite sample holders. Samples were supported on the distal side by 0.025 mm thick mylar tape. The size of the sample holders was chosen so that they could be inserted directly into an Air Products Helitran cryostat for monitoring the EPR spectrum of the sample. All illuminations, EPR measurements, and X-ray absorption measurements were performed directly on samples mounted in these holders.

Samples were dark adapted for 1 h prior to illumination. The samples were then illuminated with a 400-W tungsten lamp through a 5-cm water filter for 90 s at 195 K in a dry ice/methanol bath contained within an optical Dewar. Sample temperature was monitored throughout with a copper–constantan thermocouple.

EPR spectra were recorded by using a Varian E109 spectrometer equipped with a Model 102 microwave bridge. Sample temperature was maintained at 8 K by using an Air Products liquid He cryostat. Spectra were recorded at 9.21 GHz with a field modulation of 32 G at 100 kHz, using a microwave power of 50 mW. The amplitude of the multiline EPR signal was quantitated by adding peak-to-trough amplitudes of four of the hyperfine lines on the low-field side of $g = 2$, measured from the illuminated-minus-dark difference spectra.

*Inorganic Manganese Compounds.* Four inorganic manganese compounds were examined in this study. The four compounds examined were $Mn^{II}Mn^{III}_2(\mu_3\text{-}O)(\text{benzoate})_6(\text{pyridine})_2(ClO_4)_2$ (**1**) (Vincent et al., 1987b), (tetra-*N*-butylammonium)$Mn^{III}_3(\mu_3\text{-}O)(\text{benzoate})_6(\text{imidazole-H})_3(ClO_4)_2$ (**2**) (G. Christou, personal communication), $Mn^{III}_4(\mu_3\text{-}O)_2(\text{acetate})_7(2,2'\text{-bipyridine})_2(ClO_4)$ (**3**) (Vincent et al., 1987a), $Mn^{II}Mn^{III}_3(\mu_3\text{-}O)_2(\text{acetate})_7(2,2'\text{-bipyridine})_2$ (**4**) (Vincent et al., 1987a). All complexes examined were synthesized and characterized in the laboratory of Dr. G. Christou. Inorganic compounds will be referred to in the text by abbreviation containing only the nuclearity and the valence [i.e., $Mn_3$(II,III,III) and $Mn_3$(III,III,III) for the trinuclear complexes and $Mn_4$(II,III,III,III) and $Mn_4$(III,III,III,III) for the tet-

ranuclear complexes]. Solid samples were diluted into an inert light element matrix ($LiBF_4$ or $Li_2CO_3$) and mounted in Lucite sample holders.

X-ray absorption spectra collected in the fluorescence mode (Jaklevic et al., 1977) were recorded at the Stanford Synchrotron Radiation Laboratory, Stanford, CA, during dedicated operation of the SPEAR storage ring, which provides 40–80-mA electron beams at 3.0 GeV. The Mn K-edge absorption spectra were obtained on the wiggler beam line IV-2 by using a Si⟨111⟩ double-crystal monochromator. Energy calibration was maintained by simultaneously measuring the strong narrow preedge feature of $KMnO_4$ at 6543.3 eV (Goodin et al., 1983). Despite a loss of a factor of about 4 in flux, EXAFS scans were recorded by using Si⟨400⟩ monochromator crystals due to the presence of variable diffraction "glitches" in the EXAFS spectra obtained with Si⟨111⟩ crystals. EXAFS spectra were recorded by using a solid-state lithium-drifted silicon X-ray detector as previously described (Jaklevic et al., 1977; Goulding et al., 1983a). The use of a triangular pulse shaping amplifier substantially improved the photon counting rate of this solid-state detection system (Goulding et al., 1983b).

X-ray absorption edge spectra were recorded by using a plastic scintillation array. Details of the design of the plastic scintillation array used in fluorescence detection of Mn K-edge absorption spectra have been described in detail previously (Yachandra et al., 1986). Samples were maintained in liquid nitrogen in the dark prior to and immediately following X-ray absorption measurements. To ensure functional integrity and confirm a stable S-state composition, EPR spectra were recorded as described above, before and after X-ray measurements. During X-ray measurements, the PSII samples mounted in Lucite sample holders were inserted into a double-wall Kapton cryostat maintained at 170 K by a liquid $N_2$ cooled $N_2$ gas flow system.

*X-ray Data Analysis.* Data analysis procedures have been described in detail elsewhere (Kirby, 1981; Goodin, 1983; Yachandra et al., 1986a). As a result, only a brief outline of data analysis procedures will be presented here. Mn K-edge spectra of PSII preparations analyzed are the sum of three or four individual scans. A linear preedge background was subtracted. The Mn K-edge energy was taken as the first major edge inflection point, determined as the maximum of the first derivative of the smoothed edge. A linear 4-eV smoothing fit was calculated for each edge. The derivative of the smoothed edge was taken as an approximation to the true first derivative. Uncertainties in the determination of the first major inflection are typically ±0.1 eV.

For EXAFS analysis, 30–40 individual scans were added after they had been examined for satisfactory signal-to-noise ratio and were determined to be free of anomalies. The EXAFS oscillations, $\chi(k)$, in the absorption cross section were obtained from the data by subtraction of a cubic spline fit to remove the free-atom absorption and any background contributions to the spectrum. Because the concentration of manganese in PSII preparations is low (approximately 500–800 $\mu$M) and as a result our signal-to-noise ratio is relatively small, we chose to multiply our data by $k^1$ to compensate for the gradual decay in the amplitude of EXAFS oscillations (EXAFS oscillations are often multiplied by $k^3$ to compensate for the approximately $1/k^3$ dependence of EXAFS oscillations beyond $k = 4$ Å$^{-1}$). Where possible, individual scattering shells were isolated by applying a window function to the Fourier transform of the EXAFS. The back-transformed data were then fit by using phase and amplitude functions which have been calculated by Teo and Lee (1979). The use of Fourier-filtered data greatly improves convergence of the nonlinear least-squares fitting procedure which yields the structural information. Four parameters are used in the simulation of each component. The distance information contained in the frequency of the EXAFS waves is determined by simulation and is in general very accurate. The accuracy is limited only by a weak correlation between the distance parameter and the assignment of the threshold for ionization. The uncertainty is typically ±0.03 Å. The number of scatterers in a given shell determines the amplitude of that wave. However, the uncertainty in the number of scatterers determined by simulation is greater than that for the distances obtained, due to a strong correlation between the degree of disorder and the number of atoms within a shell. The disorder within a scattering shell is parameterized by a Debye–Waller-like term. The error in the determination of the number of scatterers can be as large as 50% and is typically ±20% (Teo & Lee, 1979). When two unresolved components are present in a given scattering shell, additional correlations can occur between the amplitude of one component and the distance to the other which limit the accuracy of a given parameter (Eisenberger & Lengeler, 1980).

Fits to the EXAFS of the PSII preparations were performed by using constraints on the range of variation in the ionization threshold ($E_0$) which we have found yield the best agreement with the internuclear distances obtained from the crystal structures of inorganic complexes. These constraints reduced systematic errors associated with the correlation between the energy of the ionization threshold (which determines the phase and to a lesser extent the frequency of a given EXAFS wave) and the distance to a scattering shell. For example, for the Mn–Mn distances in multinuclear $\mu$-oxo-bridged complexes, agreement to within ±0.02 Å is obtained by constraining $E_0$ to the range between 6550 and 6560 eV. In all simulations an initial edge threshold of 6560 eV is assumed. The energy of the edge threshold was varied in the nonlinear least-squares minimization procedure by allowing a correction term to the initial estimate of the ionization threshold ($\Delta E_0$) to vary between 0 and −10 eV. This approach using fine adjustments based on models was developed by Teo et al. (1983).

## Results

*EPR Spectral Characterization.* Continuous illumination at 195 K of dark-adapted subchloroplast PSII membranes generates and traps a species that exhibits a multiline EPR signal (Brudvig et al., 1983). The decrease in amplitude of this signal following illumination at 195 K of PSII membranes containing low concentrations of hydroxylamine is the criterion that was used in this study to determine the fraction of centers delayed by two flashes in the S-state cycle. Centers affected in this manner are now poised in a state resembling $S_0$.

Changes in the EPR spectrum in the region around $g = 1.9$ were monitored as an indication of reduction of the primary acceptor in PSII preparations (Rutherford & Zimmermann, 1984). This signal is analogous to the reduced primary acceptor signal which has been extensively characterized in reaction center preparations from purple non-sulfur bacteria (Butler et al., 1984). de Paula et al. (1985) have used the amplitude of this signal to quantitate the relative number of stable charge separations. It is interesting to note that the $g = 2.1$ EPR signal associated with an altered configuration of the iron–quinone complex induced by low concentrations of hydroxylamine (Sivaraja & Dismukes, 1988) was not observed in our study. However, this is not surprising in light of the fact that we added DCMU prior to the addition of hydrox-

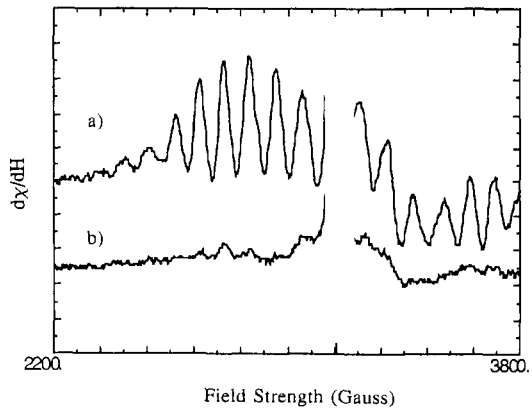


FIGURE 1: Illuminated-minus-dark difference EPR spectra of PSII preparations illuminated for 2 min at 195 K without hydroxylamine (upper trace) or containing 60 $\mu$M hydroxylamine (lower trace). Spectrometer conditions are described under Experimental procedures.

ylamine in order to ensure that the PSII reaction center was limited to a single turnover at the illumination temperature examined. DCMU has been shown to inhibit the formation of the $g = 2.1$ EPR signal (Sivaraja & Dismukes, 1988). Figure 1 contains the illuminated-minus-dark X-band EPR spectra recorded at 8 K of two preparations: (a) a dark-adapted PSII sample that was illuminated at 195 K for 90 s and (b) a PSII sample that was treated in the same manner but also contained 60 $\mu$M hydroxylamine. The amplitude of the residual multiline EPR signal exhibited by the hydroxylamine-treated sample is <5% of the control $S_2$ sample. The amplitude of the reduced primary acceptor signal shown in Figure 1a was estimated by comparing the amplitude of the second manganese hyperfine feature on the high-field side of $g = 2$ in the multiline spectrum presented here with that from a multiline spectrum which is not convolved with the reduced quinone acceptor signals (e.g., the 8 K EPR spectrum of a PSII preparation containing 1 mM PPBQ which was illuminated at 195 K and warmed for 30 s at 293 K, data not shown). On the basis of this estimate, the amplitude of the $g = 1.9$ feature in the difference EPR spectra of both samples is approximately the same. This was taken as an indication of stable charge separation and the storage of an oxidative equivalent on the donor side of PSII in both cases. As a byproduct of the oxidation of $Q_{400}$, an extremely stable charge-separated state (in this case the $S_2$ state) is generated by illumination at 195 K of PSII preparations containing 1 mM PPBQ followed by warming for 30 s at 293 K (Zimmermann & Rutherford, 1986; Petrouleas & Diner, 1987). The warming step results not only in the oxidation of $Q_{400}$ but also in the complete oxidation of the reduced primary quinone acceptor.

*Mn K-Edge X-ray Absorption Spectra.* Mn K-edge X-ray absorption studies were performed on samples poised predominantly in the $S_1$·$NH_2OH$, $S_0$*, $S_1$, and $S_2$ states. Signal-averaged Mn K-edge X-ray absorption spectra of PSII samples poised in the $S_1$·$NH_2OH$ and the $S_1$ states are shown in Figure 2. The $S_1$·$NH_2OH$ spectrum, shown in Figure 2, is that of a dark-adapted PSII preparation incubated with 40 $\mu$M hydroxylamine. Within the signal-to-noise and the uncertainty of the measured-edge inflection energies, these two spectra are identical. Changes in the edge position would reflect oxidation-state changes. Changes in the symmetry of the site accompanying a conformational change within the manganese cluster would be indicated by changes in the shape and/or position of the edge [for a review, see Srivastava and Nigam (1972)]. The absence of such changes indicates that PSII preparations poised in the the $S_1$ state and the dark-

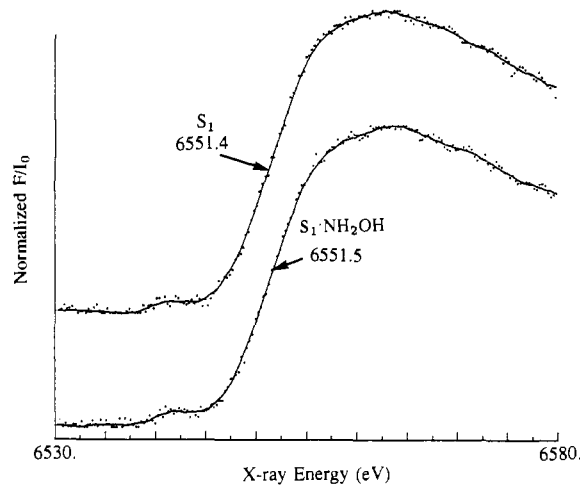


FIGURE 2: Comparison of the Mn K-edge absorption spectra of dark-adapted PSII samples with ($S_1$·$NH_2OH$) or without ($S_1$) hydroxylamine. Within the signal-to-noise and the uncertainty of the edge measurement, the spectra of the PSII samples poised in the $S_1$ and $S_1$·$NH_2OH$ states are identical. A linear fit to the spectrum below the onset of Mn absorption has been removed. The data were collected in fluorescence mode and were ratioed to the incident X-ray photon intensity, $I_0$. Normalized fluorescence counts, $F/I_0$, are plotted as a function of X-ray photon energy in electronvolts. Smoothed curves have been drawn through the data points. A running quadratic fit with a 2-eV domain was used to smooth the data for presentation.

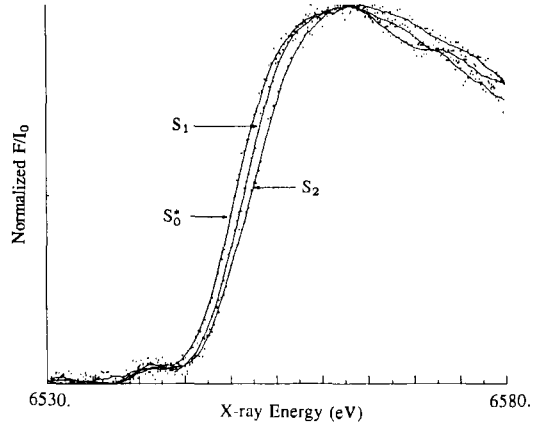


FIGURE 3: Comparison of the Mn K-edge absorption spectra of PSII preparations poised in the $S_0$*, $S_1$, and $S_2$ states of the oxygen-evolving complex. Spectra shown are the Mn X-ray absorption edges of a dark-adapted PSII preparation ($S_1$), a PSII preparation illuminated at 195 K ($S_2$), and a PSII preparation containing 40 $\mu$M hydroxylamine illuminated at 195 K ($S_0$*). Spectra are plotted as described in Figure 2.

adapted preparations treated with hydroxylamine contain manganese complexes at the same oxidation level and that the site symmetry is unaltered. This is direct spectroscopic evidence that hydroxylamine at the concentrations which induce a two-state delay in the catalytic cycle does not cause reduction of the manganese center in the dark.

Signal-averaged Mn K-edge spectra of the $S_0$*, $S_1$, and $S_2$ states are shown in Figure 3. The Mn K-edge of the $S_0$* preparation shown is that of a PSII sample treated with 40 $\mu$M hydroxylamine and illuminated at 195 K. A shift to lower energy upon illumination of hydroxylamine-containing samples is observed. This shift is comparable in magnitude but opposite in sign to the light-induced shift that we have previously reported for the $S_1 \rightarrow S_2$ state transition (Yachandra et al., 1986a). The shifts that we observed for the $S_1 \rightarrow S_2$ and $S_1 \rightarrow S_0$* states are comparable in magnitude to the shift observed when a single electron is removed from a binuclear manganese complex; however, similar shifts are also observed when a single

Table I: Mn K-Edge Inflection Energies of PSII Preparations Treated with Hydroxylamine

| hydroxylamine concentration ($\mu$M) | sample treatment | multiline signal amplitude[a] | state composition | $Mn^{2+}$ content[b] (%) | Mn K-edge energy (eV) |
|---|---|---|---|---|---|
| 0 | dark adapted | 0 | 100% $S_1$ | 5 | 6551.4 |
| 0 | illuminated, 195 K | 100 | 100% $S_2$ | 5 | 6552.3 |
| 40 | dark adapted | 0 | 35% $S_1$·$NH_2OH$, 65% $S_1$ | 5 | 6551.5 |
| 40 | illuminated, 195 K | 35 | 35% $S_2$, 65% $S_0$* | 5 | 6550.2 |
| 60 | dark adapted | 0 | 93%[c] $S_1$·$NH_2OH$ | 12 | 6550.6 |
| 60 | illuminated, 195 K | 0 | 93% $S_0$* | 12 | 6549.9 |
| 100 | dark adapted | 0 | 84% $S_1$·$NH_2OH$ | 21 | 6549.9 |
| 100 | illuminated, 195 K | 0 | 84% $S_0$* | 21 | 6549.5 |

[a] Multiline signal amplitudes are expressed as percentages of those of the control (0 $\mu$M $NH_2OH$) $S_2$ state sample which was generated by illumination at 195 K. [b] $Mn^{2+}$ content is expressed as a percentage of the total manganese present, as determined by atomic absorption. Uncertainties in the $Mn^{2+}$ concentration are estimated to be ±3%. [c] Reductions in the state composition from 100% are based on the release of $Mn^{2+}$ above the control levels.

electron is removed from a tetranuclear manganese complex (Guiles, 1988).

Table I contains the multiline EPR signal amplitudes, the estimated state composition, and Mn K-edge inflection energies for a set of hydroxylamine-treated PSII preparations. Three hydroxylamine concentrations were examined: 40, 60, and 100 $\mu$M. All PSII preparations containing hydroxylamine exhibited a light-induced shift to lower X-ray edge energy. The most straightforward interpretation of this result is that, upon illumination, reduction of the manganese center occurs.

Qualitatively, the manganese K-edge energy increases with increasing oxidation state. However, the position of the K-edge is actually an indication of the positive potential of the metal center and is, thus, also affected by the electron-donating character of ligand atoms. The manganese K-edge energy of the $S_0$* state is roughly in the range of edge energies associated with a formal valence of Mn(III) (Kirby et al., 1981a; Sauer et al., 1988; Guiles, 1988).

A shift to lower X-ray edge energy occurs in dark-adapted preparations containing higher concentrations (60 $\mu$M) of hydroxylamine, relative to dark-adapted samples which do not contain hydroxylamine. The magnitude of this shift increases with increasing hydroxylamine concentration. Also contained in Table I is the fraction of the total manganese present as $Mn^{2+}$ as determined by the amplitude of the six-line EPR spectrum recorded at 8 K. Total manganese present was determined by atomic absorption. The magnitude of the dark shift in the Mn K-edge inflection energy correlates with the amount of $Mn^{2+}$ released. A shift of ~0.5 eV occurs for each increment of 10% of the total manganese released as $Mn^{2+}$. Simulations performed by adding a fraction of the X-ray absorption edge of hexaaquo $Mn^{2+}$ to the $S_1$ edge as indicated in Table I yield decreases in the X-ray edge energy, relative to that of $S_1$, consistent with the observed behavior. Hydroxylamine at higher concentrations is known to release manganese in the form of $Mn^{2+}$ (Cheniae & Martin, 1970; Tamura & Cheniae, 1985). The release of $Mn^{2+}$ has been found to be strongly correlated with the loss of oxygen-evolving activity (Cheniae & Martin, 1970; Tamura & Cheniae, 1985). The lowest concentration of hydroxylamine, which induces a light-induced edge shift, does not result in a shift to lower edge energy in the dark, relative to controls that do not contain hydroxylamine. This indicates that the dominant reaction leading to the two-state delay in the S-state cycle, which occurs at low concentrations of hydroxylamine, is due to a light-induced reduction of the manganese center. The dark reactions which increase with increasing hydroxylamine concentration reflect only a small fraction of the centers present. The manganese released is in the form of nonfunctional $Mn^{2+}$.

*Mn EXAFS Analyses.* The $k^1$-weighted EXAFS modulations of a $S_0$* sample are shown in Figure 4 together with the $k^1$-weighted EXAFS spectrum of an $S_1$ sample. Differences in the EXAFS waves are evident. Also, the amplitude of the oscillations in the EXAFS of the PSII preparation in the $S_1$ state is significantly greater than those of the $S_0$* state. Figure 5a contains the Fourier transforms of the $k^1$-weighted EXAFS of Mn in the $S_0$* and $S_1$ states. Two major peaks are evident in the Fourier transforms of both PSII preparations. Note that the apparent distances to the scattering shells in Figure 5 are shorter than the actual distances to neighboring atoms. This is due to the fact that the radial distribution function, $R'$, obtained by Fourier transforming an EXAFS spectrum yields distances that are convolved with an averaged phase shift. This phase shift is characteristic of the absorbing atom–scattering atom pair. This complication, which tends to decrease the apparent distance, is actually useful in that it is indicative of the nature of the scattering atom.

The amplitudes of the peaks in the Fourier transform of the $S_0$* Mn EXAFS are substantially lower than those of the corresponding peaks in the $S_1$ state EXAFS Fourier transform.

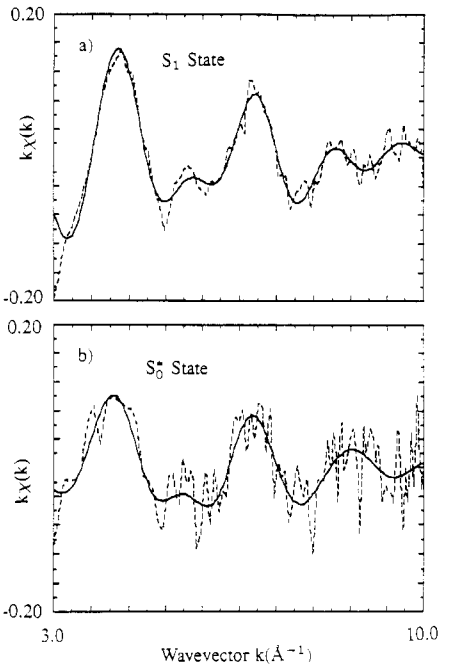


FIGURE 4: $k^1$-weighted EXAFS region of the Mn X-ray absorption spectrum of (a) a dark-adapted PSII preparation (e.g., a $S_1$ state preparation) and (b) a PSII preparation poised in the $S_0$* state. The $S_0$* state sample contained 60 $\mu$M hydroxylamine. The EPR spectrum of this sample is shown in Figure 1. The EXAFS data are indicated with a dashed line, and the solid trace is the sum of the Fourier components due to the two main peaks in the Fourier transform of the EXAFS spectra shown in Figure 5.

Table II: Simulation Results for the First Coordination Sphere of PSII Preparations Poised in the $S_1$ and $S_0$* States;[a] $k^1$-Weighted EXAFS Data

| | Mn–O (bridging ligands) | | | | Mn–O or –N (terminal ligation) | | | | |
|---|---|---|---|---|---|---|---|---|---|
| preparation | $N$[b] | $R$ (Å)[c] | $\sigma^2$ (Å$^2$)[d] | $\Delta E_0$[e] | $N$ | $R$ (Å) | $\sigma^2$ (Å$^2$) | $\Delta E_0$ | $F$[f] |
| $S_1$ | 1.5 | 1.76 | 0.005 | −20 | 4.4 | 2.25 | 0.028 | −20 | 0.0066 |
| $S_0$* | 1.6 | 1.79 | 0.004 | −16 | 2.3 | 2.20 | 0.023 | −20 | 0.0026 |

[a] Simulations were performed using theoretically calculated phase shift and backscattering amplitude functions calculated by Teo and Lee (1979). [b] $N$ is the number of neighboring atoms, which is adjusted from the value obtained by simulation by a factor of 2 (Teo & Lee, 1979). [c] $R$ is the internuclear distance between the absorbing Mn atom and the neighboring atom. [d] $\sigma$ is the Debye–Waller parameter, equal to the root-mean-square sum of static and dynamic disorder in the internuclear distance, $R$. [e] The X-ray ionization threshold, $E_0$, is also allowed to vary from an initial value. In all cases the initial value of the ionization threshold was assumed to be 6560 eV. The parameter $\Delta E_0$ was constrained to −20 to 0 eV. [f] The goodness of fit criterion is a least-squares residual, $F$, between the Fourier-isolated waves (see caption of Figure 6) and the simulation of these waves.

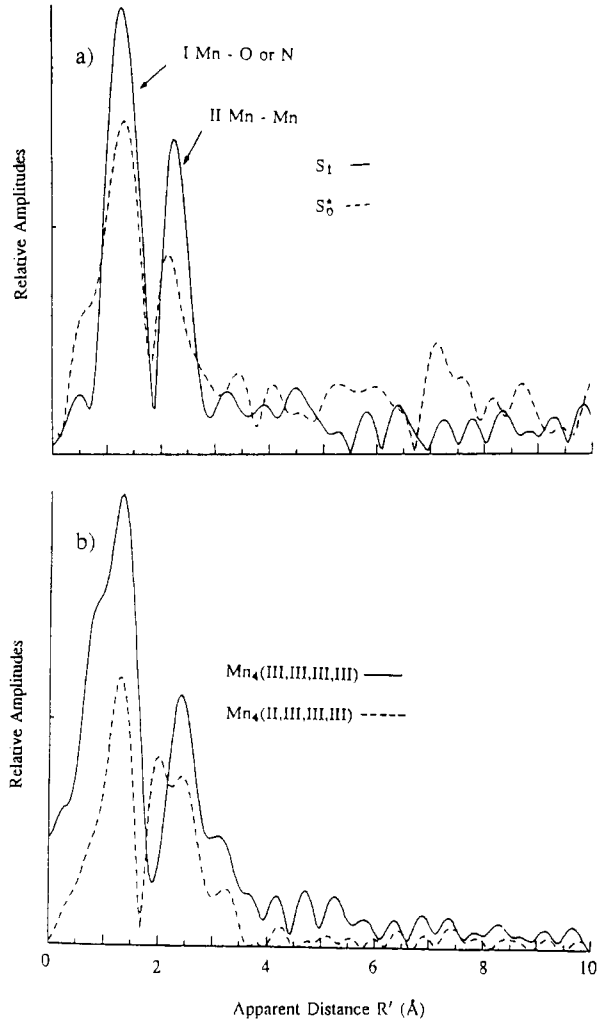


FIGURE 5: (a) Fourier transforms of the $k^1$-weighted Mn EXAFS of an $S_1$ state preparation (—) and an $S_0$* state preparation (---). Spectra plotted are the Fourier transforms of the Mn EXAFS spectra (dashed lines) shown in Figure 4. The significantly lower amplitude of the $S_0$* state preparation Mn EXAFS peaks indicates a much more disordered system. The distances to each scattering shell are shorter than the true bond lengths due to an average phase shift, $\langle d\alpha(k)/dk\rangle_k$, which is characteristic of the given absorber–scatterer pair. (b) The Fourier transforms of the $k^1$-weighted Mn EXAFS of a tetranuclear manganese compound $[Mn^{III}_4(\mu_3\text{-O})(acetate)_7(2,2'\text{-bipyridine})_2(ClO_4)]$ is indicated with the solid trace. Also plotted, with a dashed line, is the Fourier transform of an isostructural manganese tetranuclear complex $[Mn^{II}Mn^{III}_3(\mu_3\text{-O})(acetate)_7(2,2'\text{-bipyridine})_2]$ which contains one Mn(II) ion not present in the former isostructural complex. Note that the reduction in the amplitude of the Fourier peaks is remarkably similar to that observed between the $S_1$ and $S_0$* states.

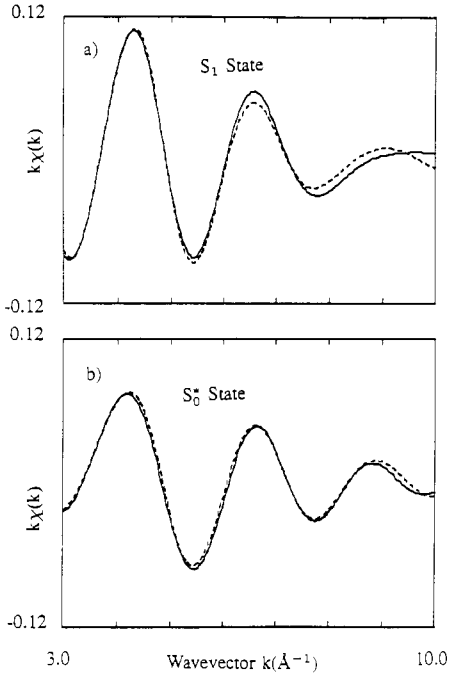


FIGURE 6: The lowest frequency component, or first shell, of the $k^1$-weighted Mn EXAFS of PSII preparations poised in the $S_1$ and $S_0$* states. This low-frequency component is obtained by multiplying the Fourier transformed data by a function that isolates the peak in the Fourier transform which occurs at the shortest distance. This spectrum is then back-transformed to yield the solid traces which are simulated by using theoretically calculated amplitude and phase functions. The best fits to the "Fourier-isolated" EXAFS are indicated by the dashed traces. The spectra shown in (a) are of the EXAFS of an $S_1$ state preparation, and the spectra in (b) are the EXAFS of an $S_0$* state PSII preparation. Simulation parameters for the fits shown are contained in Table II.

This change is characteristic of an increase in the disorder present in the distances to both scattering shells. Similar behavior has been observed with increasing temperature in other systems (Brown & Eisenberger, 1979; Scott et al., 1986). We have observed similar reductions in the amplitude of Fourier peaks of multinuclear manganese compounds that have been chemically reduced. For example, Figure 5b contains the Fourier transforms of two isostructural tetranuclear manganese compounds that differ in formal valence. The lower amplitude Fourier peaks indicated by the dashed trace are those of the more reduced complex $[Mn_4(II,III,III,III)]$ which contains one Mn(II) ion not present in the other complex.

Figure 6 presents the EXAFS oscillations due to backscattering from the first coordination sphere of the manganese complex in $S_0$* and $S_1$ state preparations together with simulations of the spectra based on theoretical phase and amplitude functions calculated by the method of Teo and Lee (1979). The $S_0$* preparation EXAFS spectrum shown is of a sample prepared by incubation with 60 $\mu$M hydroxylamine. The illuminated-minus-dark EPR spectrum of this sample is shown in Figure 1b. The Fourier-filtered data shown are a composite of the Fourier components which yield the peak labeled I in the Fourier transform. Table II contains a summary of the results obtained from simulations of the first

Table III: Simulation Results for the Second Shell of PSII Preparations Poised in the $S_1$ and $S_0$* States;[a] $k^1$-Weighted EXAFS Data

| | Mn–Mn | | | | Mn–C | | | | |
|---|---|---|---|---|---|---|---|---|---|
| state | $N$ | $R$ (Å) | $\sigma^2$ (Å$^2$) | $\Delta E_0$ | $N$ | $R$ (Å) | $\sigma^2$ (Å$^2$) | $\Delta E_0$ | $F$[b] |
| $S_1$ | 1.1 | 2.74 | 0.005[c] | −6 | 1.8 | 3.18 | 0.010[c] | −18 | 0.00067 |
| $S_0$* | 1.0 | 2.71 | 0.011 | −10 | 0.8 | 3.26 | 0.010[c] | −20 | 0.0054 |
| | Mn–Mn | | | | Mn–Mn | | | | |
| state | $N$ | $R$ (Å) | $\sigma^2$ (Å$^2$) | $\Delta E_0$ | $N$ | $R$ (Å) | $\sigma^2$ (Å$^2$) | $\Delta E_0$ | $F$[b] |
| $S_1$ | 0.8 | 2.67 | 0.005[c] | −9 | 0.9 | 2.79 | 0.005[c] | −7 | 0.0018 |
| $S_0$* | 1.0 | 2.69 | 0.005[c] | −10 | 0.5 | 2.87 | 0.005[c] | −10 | 0.0026 |

[a] Simulations were performed using theoretically calculated phase shift and backscattering amplitude functions calculated by Teo and Lee (1979). [b] The quality of the fit is indicated by a least-squares residual, $F$, between the Fourier-isolated waves (see caption of Figure 6) and the curve obtained by simulation of these waves. [c] The Debye–Waller factors used in these simulations were constrained to reasonable values (Guiles et al., 1989). Left unconstrained, these parameters floated to unreasonably low or high values.

coordination sphere of the manganese EXAFS of the $S_0$* and the $S_1$ state PSII preparations. The presence of two unresolved components is clearly revealed. The least-squares residual, $F$, improves by more than an order of magnitude upon the addition of a second EXAFS component. The two components obtained are quite reasonable in light of what is known about the first coordination sphere of $\mu$-oxo-bridged multinuclear manganese complexes. The shorter, less disordered oxygen shell at 1.8 Å corresponds to the bridging oxygens, while the longer more disordered shell corresponds to the terminal ligation shell which is typically more disordered in Mn(III) complexes due to Jahn–Teller distortions (Plaksin et al., 1972; Stebler et al., 1986; Sheats et al., 1987; Vincent et al., 1987).

The quality of the simulation of the first shell EXAFS of $S_0$* data is significantly better than that obtained for the first shell of the $S_1$ data. This may indicate that first coordination sphere distances in the $S_0$* are a more continuous distribution of bond lengths which is more accurately modeled by a single scattering shell with a bond length distribution approximated by a Gaussian Debye–Waller term than is the distribution of distances present in the $S_1$ state. Despite the reduction in amplitude of the Fourier peak corresponding to the first shell EXAFS of the $S_0$* state relative to that of the $S_1$ state, the Debye–Waller terms for the first shell EXAFS of the $S_0$* state determined by fitting the data indicate a slight decrease in the disorder in Mn–O or –N distances relative to that of the $S_1$ state sample. This erroneous counterintuitive fitting behavior has been observed before in other disordered systems (Eisenberger & Lengeler, 1980).

Figure 7 shows that EXAFS oscillations due to the second shell scatterers in PSII preparations poised in the $S_0$* and $S_1$ states. We have previously shown that the $k$-weighting behavior of the second shell of $S_1$ state preparations indicates the presence of a heavy scatterer like manganese (Kirby et al., 1981b; Yachandra et al., 1986a). Simulations of the second shell scatterers indicate that this shell also is heterogeneous. Simulations using two components, a manganese scatterer and a carbon shell or two different manganese neighbors, improve the fit quality by a factor of as much as 3. Unlike the first shell, the origin of the heterogeneity in the second shell is less clear. An examination of second shell distances in the crystal structures of multinuclear oxo-bridged manganese complexes with biomimetic ligands, such as carboxylates or heterocyclic rings, indicates that the second shell scatterers of the manganese in PSII must also contain some carbon atoms. In addition, it is generally accepted that there are four manganese per PSII reaction center (Kuwabara & Murata, 1984; Govindjee et al., 1985); thus, it is reasonable to consider heterogeneity in the Mn–Mn distance arising from two inequivalent dimers or due to distortions in a higher nuclearity complex. Thus, two models of the heterogeneity in

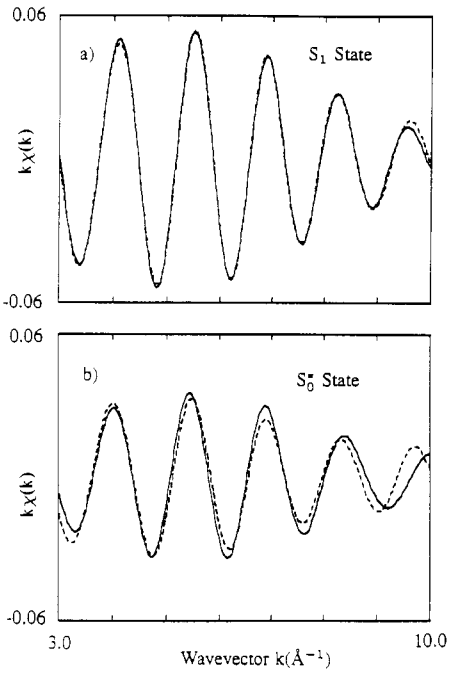


FIGURE 7: Fourier isolates (—) and fits (- - -) to the second shell of the $k^1$-weighted EXAFS of PSII preparations poised in the $S_1$ (a) and $S_0$* (b) states. The simulations plotted are two-component simulations assuming a Mn–Mn wave and a Mn–C wave. The results obtained from the simulations shown are contained in Table III.

the second shell were assumed, each containing two components as described. Table III contains the best fit parameters for the second shell of PSII preparations poised in the $S_0$* and $S_1$ states, assuming the following scattering shell models: (1) one manganese neighbor and a carbon shell and (2) two different manganese neighbors. It is important to note that the apparent spread in Mn–Mn distances determined from the two manganese neighbor simulation is greater in the $S_0$* state preparation (e.g., 0.18 Å for $S_0$* compared to 0.12 Å for the $S_1$).

Note that, for the $S_1$ state preparation, the Debye–Waller term has been constrained to a reasonable value (Guiles et al., 1990). It is is clear from the alteration in both the envelope shape and amplitude of the second shell EXAFS of the $S_0$* state preparation that the disorder present in this shell is significantly higher than that present in the $S_1$ state EXAFS. Note that the increase in the spread of Mn–Mn distances indicated by the Debye–Waller terms (e.g., 0.03 Å) is somewhat smaller than the increased spread indicated by the two Mn–Mn shell simulations.

## Discussion

*The Mechanism of Action of Hydroxylamine.* The striking

Scheme II

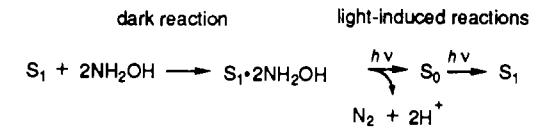


similarity of the Mn K-edge of dark-adapted PSII samples containing low concentrations of hydroxylamine ($S_1$·$NH_2OH$ state samples) or without hydroxylamine ($S_1$ state samples) is spectroscopic evidence that manganese is not reduced by hydroxylamine in the dark. Thus, the first two mechanisms described in Scheme I may be ruled out.

The simplest interpretation of the light-induced shift to lower energy observed in samples treated with hydroxylamine is that, concurrent with turnover of PSII, hydroxylamine induces a two-electron reduction of the oxygen-evolving complex relative to that of the $S_2$ state. This is indicated by the following facts. The inflection points of the Mn K-edge of the dark-adapted PSII membrane suspensions with or without hydroxylamine present are at the same energy, indicating that the oxidation state of the manganese complex in the OEC is the same for $S_1$·$NH_2OH$ and $S_1$. In the absence of hydroxylamine, the Mn K-edge inflection of preparations that have been illuminated at 195 K shifts to higher energy by approximately 1 eV (Goodin et al., 1984; Yachandra et al., 1987; McDermott et al., 1988). The magnitude of the shift in edge inflection energy observed upon illumination of PSII preparations containing hydroxylamine is comparable in magnitude but opposite in sign to that we observed for samples that do not contain hydroxylamine. Thus, the edge inflection energy of an $S_0$* preparation is nearly 2 eV lower than that of the state (the $S_2$ state) that would have been generated by continuous illumination at 195 K of samples which do not contain hydroxylamine. This implies that the reduction induced by illumination of PSII preparations containing hydroxylamine is a two-electron transfer from hydroxylamine resulting in the generation of the $S_0$ state and the production of dinitrogen, two protons, and two water molecules as depicted in eq 1. The net reaction

$$2NH_2OH \rightarrow 2e^- + N_2 + 2H^+ + 2H_2O \qquad (1)$$

describing this proposed mechanism is depicted in Scheme II. Note that it seems probable that at least transient generation of the $S_2$ state initiates the proposed two-electron reduction of the manganese complex in the presence of hydroxylamine.

Förster and Junge (1985a) examined the effect of hydroxylamine on the flash-induced proton-release pattern observed in whole chloroplasts using absorption changes of methyl red. The flash pattern of protons released in the presence of hydroxylamine matches the normal pattern but is delayed by two flashes. The amplitude of the absorption change on the first flash was consistent with the release of two protons. Junge and Förster (1985b) speculated that these two protons are the product of the oxidation of two molecules of hydroxylamine. Alternatively, it has been suggested that these two protons are the result of the subsequent binding and hydrolysis of two water molecules at the water oxidation site (Andrëasson et al., 1983). More recently, it was suggested, on the basis of mass spectrometric measurements with $^{18}O$-labeled water, that the substrate water does not bind irreversibly to the OEC until the $S_3 \rightarrow S_4$ state transition (Radmer & Ollinger, 1986). This lends more credence to the assertion that two protons released after the first flash in the presence of hydroxylamine are the result of oxidation products of two molecules of hydroxylamine. On the basis of this assertion, Förster and Junge (1986) proposed a model in which hydroxylamine causes a two-electron reduction of the manganese complex upon advancement to the $S_2$ state (see Scheme II and eq 1). These results are consistent with our assertion of a light-induced hydroxylamine-mediated two-electron transfer to the PSII reaction center.

Förster and Junge (1985c) also found that the effect of hydroxylamine was reversible in the dark with a half-time to maximum effect on the order of 1 min. This reversibility of hydroxylamine binding would seem to argue against dark reduction of the oxygen-evolving complex. On the basis of an observed sigmoidicity in the methyl red absorption changes occurring on the first flash with increasing hydroxylamine concentration, Förster and Junge (1985c) concluded that as many as four molecules of hydroxylamine bind cooperatively to the oxygen-evolving complex. On the basis of this observation, Förster and Junge (1986) proposed a model in which serial bridged binding of hydroxylamine to a binuclear manganese center induces a significant increase in the manganese–manganese distance. The small changes that we have observed within the binuclear manganese core structure rule out the possibility of a large conformational change due to bridged binding of hydroxylamine at manganese. The observed cooperativity and reversibility of the effect have been independently confirmed by Diedrich-Glaubitz et al. (1987) using inside-out thylakoids and bromocresol purple absorption changes.

Recently, Beck & Brudvig (1987) suggested that a two-electron reduction of the oxygen-evolving complex to an $S_{-1}$ state occurs at higher concentrations ($\geq$200 $\mu$M) of hydroxylamine in the dark. At these concentrations of hydroxylamine reversible inhibition of oxygen evolution occurs. Our evidence (i.e., the lack of a difference in the Mn K-edge energy of samples poised in the $S_1$·$NH_2OH$ and $S_1$ states) is inconsistent with the assertion of an intermediate two-electron reduction process occurring in the dark at the concentrations examined. However, the differences may be due to the differences in hydroxylamine concentration used and the duration of incubation.

Using a mass spectrometer equipped with a gas-permeable silicone membrane, Radmer and Ollinger (1982) investigated the flash-induced evolution of volatile molecules from chloroplasts in the presence of hydroxylamine at concentrations that alter the normal cycle of water oxidation. They found nitrogen to be the only stable oxidation product other than oxygen. The nitrogen evolved upon a series of flashes was found to be maximum on the first flash. This surplus of nitrogen evolved on the first flash was assumed to be the product of hydroxylamine oxidation at the water oxidation site. The simplest explanation of the evolution of nitrogen from active centers, consistent with the proton release pattern and our Mn K-edge results indicating that manganese is not reduced in the dark, is a concerted irreversible oxidation of two molecules of hydroxylamine occurring upon illumination as depicted in Scheme II. Presumably, this process would leave the oxygen-evolving complex in a state indistinguishable from the $S_0$ state.

*Relevance of the Properties of $S_0$* to the Native $S_0$.* When PSII preparations containing substantial $S_0$ state composition at the chlorophyll concentrations required by EXAFS experiments are prepared, we will be able to determine if the Mn complex in the state induced by hydroxylamine at low concentrations is structurally similar to the native $S_0$ state. Nonetheless, there are a number of spectroscopic studies which suggest that the hydroxylamine-induced state and the native $S_0$ state are similar. By examining the effect of hydroxylamine

on the UV absorption changes accompanying S-state transitions, Witt et al. (1987) have attempted to address this question. Their observations concur with those of Dekker et al. (1984) in that UV absorption changes which they assign to a change in the oxidation state of manganese occur during the $S_0 \rightarrow S_1$, $S_1 \rightarrow S_2$, and $S_2 \rightarrow S_3$ transitions and are reversed on the $S_3 \rightarrow (S_4) \rightarrow S_0$ transition. Unlike the difference spectra originally reported by Dekker et al. (1985), the spectrum reported by Witt et al. (1987) for the hydroxylamine-induced $S_0$ to $S_1$ transition has a maximum at 300 nm, significantly shifted from the maximum observed in the difference spectrum for the $S_1 \rightarrow S_2$ and $S_2 \rightarrow S_3$ state transitions. Witt et al. (1987) speculate that the differences between the different state transitions may reflect an oxidation-state change corresponding to Mn(II) to Mn(III) for the $S_0 \rightarrow S_1$ state transition and a Mn(III) to Mn(IV) oxidation-state change corresponding to the $S_1 \rightarrow S_2$ and $S_2 \rightarrow S_3$ state transitions. Although they do not report a complete spectrum for the calculated four-flash-induced $S_0 \rightarrow S_1$ difference spectrum, they claim that the calculated changes at 300 nm agree with the difference spectrum of the hydroxylamine-induced $S_0 \rightarrow S_1$ state transition. More recent work from the same laboratory (Kretschmann et al., 1988) has determined that the $S_0 \rightarrow S_1$ state transition exhibits optical difference spectra that are significantly different from the $S_1 \rightarrow S_2$ and $S_2 \rightarrow S_3$ state transition and conclude that the difference is probably due to a Mn(II) $\rightarrow$ Mn(III) valence change for the $S_0 \rightarrow S_1$ state transition as previously described by Witt et al. (1987). On the basis of optical difference spectra between mixed valence multinuclear manganese complexes, Vincent and Christou (1986) suggest the assignment of a Mn(II) to Mn(III) oxidation state change during the $S_0 \rightarrow S_1$ state transition.

The similarity of the hydroxylamine-induced $S_0$ state and the three-flash-induced $S_0$ state has also been examined by observing the flash-induced changes in proton relaxation properties (Srinivasan et al., 1986). The generation of a paramagnetic center with a high proton relaxation efficiency after the first flash in the presence of hydroxylamine correlated well with the generation of this species after three flashes in the absence of hydroxylamine. On the basis of this observation, Srinivasan et al. (1986) speculated that the proton relaxation properties of this center are what one might expect for a flash-generated Mn(II) center.

Recently, Styring and Rutherford (1987) have suggested that the equilibrium between $S_0$ and $D^+$, which results in the slow conversion of $S_0$ to $S_1$ in the dark, is a process that prevents the loss of manganese present in the $S_0$ state. On the basis of the fact that Mn(II) exhibits faster ligand exchange rates and, thus, is more labile, Styring and Rutherford suggested that the $S_0$ state contains at least one Mn(II) ion. If we assume that $S_0$ and $S_0$* are the same, then our proposed irreversible mechanism of hydroxylamine oxidation indicates that the $S_0^* \rightarrow S_1$ transition involves the stabilization and storage of a single oxidative equivalent at the manganese cluster. We have previously shown that there are no significant structural changes occurring in the $S_1 \rightarrow S_2$ state transition despite the clear change in oxidation state (Yachandra et al., 1987). On the basis of our X-ray edge and EXAFS results for the $S_0$* and $S_1$ states, the $S_0 \rightarrow S_1$ state transition appears to involve both an oxidation-state change from Mn(II) to Mn(III) and a structural rearrangement consistent with that change. This conclusion is consistent with the assertions by Witt et al. (1987), Srinivasan and Sharp (1986), and Styring and Rutherford (1987) described above.

The energy of the Mn K-edge inflection of the $S_0$* preparations is roughly in the range of Mn(III) complexes. However, the $S_0$* edge energy is less than 1 eV above multinuclear $\mu$-oxo-bridged manganese complexes that contain one manganese with a formal valence of II (Guiles, 1988). This difference in edge inflection energy could be due to a larger percentage of oxygen donor groups, such as carboxylates, in the coordination sphere of the manganese cluster in PSII. Note that the energy of the Mn K-edge inflection of the $S_2$ state is also higher than one would expect for the mixed valence state that the EPR properties indicate it must be (Sauer et al., 1988).

Recently, Vincent et al. (1987b) have synthesized and obtained X-ray crystal structures for a set of triangular trinuclear manganese complexes which have a formal valence of $Mn_3$(II,III,III) and $Mn_3$(III,III,III). They found a Mn–Mn distance in the $Mn_3$(II,III,III) complex 0.1 Å longer than the corresponding distance in the $Mn_3$(III,III,III) complex. Similar changes in the static disorder in the Mn–Mn distances have also been observed for isostructural pairs of tetranuclear Mn complexes (Vincent et al., 1987a). Differences in the amplitude of peaks in the Fourier transforms of these isostructural models are remarkably similar to the differences that we have observed between the Fourier transforms of the EXAFS of $S_0$* and $S_1$ state preparations (compare panels a and b of Figure 5). Conversely, differences in the EXAFS of isostructural binuclear complexes (e.g., the di-$\mu$-oxo-bridged binuclear manganese phenanthroline complexes) which differ by one oxidative equivalent but involve only the higher valences [e.g., Mn(III) and Mn(IV)] have been found to be negligibly small (Kirby et al., 1981b). An X-ray crystallographic study of this pair of binuclear complexes has confirmed the structural homology (Stebler et al., 1986). Wieghardt et al. (1986) have observed similarly small changes in structure between a pair of binuclear structures that differ by one unit of valence and involve only Mn(III) and Mn(IV). This suggests that the larger apparent spread in the Mn–Mn distances, indicated by the two Mn shell simulations of the $S_0$* state Mn EXAFS, may be due the presence of one manganese with a formal valence of Mn(II).

## Conclusions

(1) Hydroxylamine does not reduce the manganese complex in PSII in the dark at the concentrations that cause a two-state delay in the S-state cycle. (2) The reduction of the manganese complex following a single turnover of PSII is consistent with a model of the action of hydroxylamine in which irreversible oxidation of two molecules of hydroxylamine results in the production of dinitrogen, the release of two protons, and the generation of the $S_0$ state of the oxygen-evolving complex. (3) The lower Mn K-edge of the oxygen-evolving complex and the higher disorder in the bond lengths in the $S_0$* state together imply a heterogeneous mixture of valences including one Mn(II).

## Acknowledgments

We thank Dr. G. Christou for generous gifts of the inorganic compounds examined in this study. We are grateful to Dr. Joseph Jaklevic for assistance with the solid-state X-ray detection system used in the collection of the Mn EXAFS. We thank Dr. Jean-Luc Zimmermann and Vickie DeRose for reading the manuscript and for assistance in data acquisition. We thank Dr. Gary Brudvig for providing a manuscript prior to publication. We would also like to thank the staff at the Stanford Synchrotron Radiation Laboratory for their assistance.

**Registry No.** Hydroxylamine, 7803-49-8.

## REFERENCES


Andrêasson, L. E., Hansson, Ö., & Vänngård, T. (1983) *Chem. Scr. 21*, 71–74.

Babcock, G. T. (1987) in *New Comprehensive Biochemistry: Photosynthesis* (Amez, J., Ed.) pp 125–158, Elsevier, Amsterdam.

Beck, W. F., & Brudvig, G. W. (1987) *Biochemistry 26*, 8285–8295.

Beck, W. F., de Paula, J. C., & Brudvig, G. W. (1986) *J. Am. Chem. Soc. 108*, 4018–4022.

Bouges, B. (1971) *Biochim. Biophys. Acta 234*, 102–112.

Bouges-Bocquet, B. (1975) *Biochim. Biophys. Acta 292*, 772–785.

Brown, G. S., & Eisenberger, P. (1979) *Solid State Commun. 29*, 481–484.

Brudvig, G. W., Casey, J. L., & Sauer, K. (1983) *Biochim. Biophys. Acta 723*, 366–371.

Butler, W. F., Calvo, R., Fredkin, D. R., Isaacson, R. A., Okamura, M. Y., & Feher, G. (1984) *Biophys. J. 45*, 947–973.

Cammerata, K., Tamura, N., Sayre, R., & Cheniae, G. (1984) in *Advances in Photosynthesis Research* (Sybesma, C., Ed.) Vol. I, pp 311–320, Martinus Nijhoff, Dordrecht.

Cheniae, G. M., & Martin, I. F. (1970) *Biochim. Biophys. Acta 197*, 219–239.

Dekker, J. P., Van Gorkom, H. J., Wensink, J., & Ouwehand, L. (1984) *Biochim. Biophys. Acta 767*, 209–216.

de Paula, J. C., Innes, J. B., & Brudvig, G. W. (1985) *Biochemistry 24*, 8114–8120.

Diedrich-Glaubitz, R., Völker, M., Gräber, P., & Renger, G. (1987) in *Progress in Photosynthesis Research* (Biggins, J., Ed.) Vol. I, pp 519–522, Martinus Nijhoff, Dordrecht.

Dismukes, G. C., & Siderer, Y. (1981) *Proc. Natl. Acad. Sci. U.S.A. 28*, 274–278.

Eisenberger, P., & Lengeler, B. (1980) *Phys. Rev. B 21*, 4507–4520.

Förster, V., & Junge, W. (1985a) *Photochem. Photobiol. 41*, 183–190.

Förster, V., & Junge, W. (1985b) *Photochem. Photobiol. 41*, 191–194.

Förster, V., & Junge, W. (1985c) *FEBS Lett. 152*, 153–157.

Förster, V., & Junge, W. (1986) *Photosynth. Res. 9*, 197–210.

Goodin, D. B. (1983) Ph.D. Dissertation, University of California, Berkeley, CA; Lawrence Berkeley Laboratory Report No. LBL-16901.

Goodin, D. B., Yachandra, V. K., Britt, R. D., Sauer, K., & Klein, M. P. (1984) *Biochim. Biophys. Acta 767*, 209–216.

Goulding, F. S., Jaklevic, J. M., & Thompson, A. C. (1983a) LBL Technical Report No. LBL-16652, pp 1–18, University of California, Berkeley, CA.

Goulding, F. S., Landis, D. A., & Madden, N. W. (1983b) *IEEE Trans. Nucl. Sci. 30*, 301–310.

Govindjee, Kambara, T., & Coleman, W. (1985) *Photochem. Photobiol. 42*, 187–210.

Guiles, R. D. (1988) Ph.D. Thesis, University of California, Berkeley, CA; Lawrence Berkeley Laboratory Report No. LBL-25186.

Guiles, R. D., Zimmermann, J.-L., McDermott, A. E., Yachandra, V. K., Cole, J. L., Dexheimer, S. L., Britt, R. D., Wieghardt, K., Bossek, U., Sauer, K., & Klein, M. P. (1990) *Biochemistry* (preceding paper in this issue).

Hansson, Ö., Andrêasson, L.-E., & Vänngård, T. (1986) *FEBS Lett 195*, 151–154.

Jaklevic, J., Kirby, J. A., Klein, M. P., Robertson, A. S. Brown, G., & Eisenberger, P. (1977) *Solid State Commun. 23*, 679–682.

Joliot, P., Barbieri, G., & Chabaud, R. (1969) *Photochem. Photobiol. 10*, 309–329.

Kirby, J. A. (1981) Ph.D. Dissertation, University of California Berkeley, CA; Lawrence Berkeley Laboratory Report No. LBL-12705.

Kirby, J. A., Goodin, D. B., Wydrzynski, T., Robertson, A. S., & Klein, M. P. (1981a) *J. Am. Chem. Soc. 103*, 5537–5542.

Kirby, J. A., Robertson, A. S., Smith, J. P., Thompson, A. C., Cooper, S. R., & Klein, M. P. (1981b) *J. Am. Chem. Soc. 103*, 5529–5537.

Kok, B., & Velthuys, B. R. (1977) in *Research in Photobiology* (Castellani, A., Ed.) pp 111–119, Plenum Press, New York.

Kok, B., Forbush, B., & McGloin, M. (1970) *Photochem. Photobiol. 11*, 457–475.

Kretschmann, H., Dekker, J. P., Saygin, Ö., & Witt, H. T. (1988) *Biochim. Biophys. Acta 932*, 358–361.

Kuwabara, T., & Murata, N. (1984) *Plant Cell Physiol. 24*, 741–747.

McDermott, A. E., Yachandra, V. K., Guiles, R. D., Cole, J. L., Dexheimer, S. L., Britt, R. D., Sauer, K., & Klein, M. P. (1988) *Biochemistry 27*, 4021–4031.

Nugent, J. H. A. (1987) *Biochim. Biophys. Acta 893*, 184–189.

Petrouleas, V., & Diner, B. A. (1987) *Biochim. Biophys. Acta 893*, 126–137.

Plaksin, P. M., Stoufer, R. C., Mathew, M., & Palenik, G. (1972) *J. Am. Chem. Soc. 94*, 2121–2122.

Powers, L. (1982) *Biochim. Biophys. Acta 683*, 1–38.

Radmer, R., & Ollinger, O. (1982) *FEBS Lett. 144*, 162–166.

Radmer, R., & Ollinger, O. (1986) *FEBS Lett. 195*, 285–289.

Rutherford, A. W., & Zimmermann, J. L. (1984) in *Advances in Photosynthesis Research* (Sybesma, C., Ed.) Vol. 1, pp 445–448, Martinus Nijhoff, The Hague.

Sandusky, P. O., & Yocum, C. F. (1983) *FEBS Lett. 162*, 339–343.

Sandusky, P. O., & Yocum, C. F. (1984) *Biochim. Biophys. Acta 766*, 603–611.

Sandusky, P. O., & Yocum, C. F. (1986) *Biochim. Biophys. Acta 849*, 85–93.

Sauer, K., Guiles, R. D., McDermott, A. E., Cole, J. L., Yachandra, V. K., Zimmermann, J.-L., Klein, M. P., Dexheimer, S. L., & Britt, R. D. (1988) *Chem. Scr. 28A*, 87–91.

Scott, R. A., Schwartz, J. R., & Cramer, S. P. (1986) *Biochemistry 25*, 5546–5555.

Sheats, J. E., Cernuszewicz, R. S., Dismukes, G. C., Rheingold, A. L., Petrouleas, V., Stubbe, J., Armstrong, W. H., Beer, R. H., & Lippard, S. (1987) *J. Am. Chem. Soc. 109*, 1435–1444.

Shulman, R. G., Yafet, Y., Eisenberger, P., & Blumberg, W. E. (1976) *Proc. Natl. Acad. Sci. U.S.A. 73*, 1384–1388.

Sivaraja, M., & Dismukes, G. C. (1988) *Biochemistry 27*, 6297–6306.

Srinivasan, A. N., & Sharp, R. R. (1986) *Biochim. Biophys. Acta 850*, 211–217.

Srivastava, U. C., & Nigam, H. L. (1972) *Coord. Chem. Rev. 9*, 275–310.

Styring, S., & Rutherford, A. W. (1987) *Biochemistry 26*, 2401-2405.
Tamura, N., & Martin, G. (1985) *Biochim. Biophys. Acta 809*, 245-257.
Teo, B.-K., & Lee, P. A. (1979) *J. Am. Chem. Soc. 101*, 2815-2832.
Teo, B.-K., Antonio, M. R., & Averill, B. A. (1983) *J. Am. Chem. Soc. 105*, 3751-3762.
Velthuys, B., & Kok, B. (1978) *Biochim. Biophys. Acta 502*, 211-221.
Vincent, J. B., & Christou, G. (1986) *FEBS Lett. 207*, 250-252.
Vincent, J. B., Christmas, C., Huffman, J. C., Christou, G., Chang, H.-R., & Hendrickson, D. N. (1987a) *J. Chem. Soc., Chem. Commun.*, 236-238.
Vincent, J. B., Chang, H.-R., Folting, K., Huffman, J. C., Christou, G., & Hendrickson, D. N. (1987b) *J. Am. Chem. Soc. 109*, 5703-5711.
Witt, H. T., Saygin, Ö., Brettel, K., & Schlodder, E. (1987) in *Progress in Photosynthesis Research* (Biggins, J., Ed.) Vol. I, pp 523-531, Martinus Nijhoff, Dordrecht.
Yachandra, V. K., Guiles, R. D., McDermott, A., Britt, R. D., Dexheimer, S. L., Sauer, K., & Klein, M. P. (1986a) *Biochim. Biophys. Acta 850*, 324-332.
Yachandra, V. K., Guiles, R. D., Sauer, K., & Klein, M. P. (1986b) *Biochim. Biophys. Acta 850*, 333-342.
Yachandra, V. K., Guiles, R. D., McDermott, A. E., Cole, J. L., Britt, R. D., Dexheimer, S. L., Sauer, K., & Klein, M. P. (1987) *Biochemistry 26*, 5974-5981.

# Mechanisms of Mutagenesis by the Vinyl Chloride Metabolite Chloroacetaldehyde. Effect of Gene-Targeted in Vitro Adduction of M13 DNA on DNA Template Activity in Vivo and in Vitro†

J. Steven Jacobsen and M. Zafri Humayun*
*Department of Microbiology and Molecular Genetics, University of Medicine and Dentistry of New Jersey—New Jersey Medical School, 185 South Orange Avenue, Newark, New Jersey 07103*
*Received May 23, 1989; Revised Manuscript Received August 28, 1989*

ABSTRACT: 2-Chloroacetaldehyde (CAA), a metabolite of the carcinogenic industrial chemical vinyl chloride, reacts with single-stranded DNA to form the cyclic etheno lesions predominantly at adenine and cytosine. In both ethenoadenine and ethenocytosine, normal Watson–Crick hydrogen-bonding atoms are compromised. We have recently shown that CAA adduction leads to efficient mutagenesis in *Escherichia coli* predominantly at cytosines, and less efficiently at adenines. About 80% of the mutations at cytosines were C-to-T transitions, and the remainder were C-to-A transversions, a result similar to that of many noninstructional DNA lesions opposite which adenine residues are preferentially incorporated. It is widely believed that noninstructional lesions stop replication and depend on SOS functions for efficient mutagenesis. We have examined the effects of in vitro CAA adduction of the *lacZα* gene of phage M13AB28 on in vivo mutagenesis in SOS-(UV)-induced *E. coli*. CAA adduction was specifically directed to a part of the *lacZ* sequence within M13 replicative form DNA by a simple experimental strategy, and the DNA was transfected into appropriate unirradiated or UV-irradiated cells. Mutant progeny were defined by DNA sequencing. In parallel in vitro experiments, the effects of CAA adduction on DNA replication by *E. coli* DNA polymerase I large (Klenow) fragment were examined. Our data do not suggest a strong SOS dependence for mutagenesis at cytosine lesions. While adenine lesions remain much less mutagenic than cytosine lesions, mutation frequency at adenines is increased by SOS. SOS induction does not significantly alter the specificity of base changes at cytosines or adenines. The in vitro replication results show that these lesions create kinetic pause sites rather than absolute replication blocks. The simplest interpretation of the specificity of base changes is that the mechanisms of base incorporation opposite these lesions are analogous to those opposite the canonical noninstructional lesions. The high efficiency of mutagenesis opposite cytosine lesions without the aid of induced levels of SOS functions suggests that all DNA lesions lacking normal Watson–Crick base-pairing ability may nevertheless not block replication. In addition, the relatively nonmutagenic bypass of adenine lesions focuses attention on the need to understand mechanisms of error avoidance in the absence of normal base-pairing information.

Following the description of the formation of cyclic DNA lesions by the mutagen glyoxal (Shapiro, 1969), a large number of chemical carcinogens have been shown to induce such lesions. For example, 2-chloroacetaldehyde (CAA),[1] a metabolite of vinyl chloride (VC), predominantly reacts with unpaired adenine and cytosine residues to form 1,$N^6$-ethenoadenine (εA) and 3,$N^4$-ethenocytosine (εC) which are the final stable lesions derived from the dehydration of the initially

† This work was supported by USPHS Grant CA47234. M.Z.H. is the recipient of USPHS Research Career Development Award CA00907.
* Author to whom correspondence should be addressed.

[1] Abbreviations: CAA, chloroacetaldehyde; VC, vinyl chloride; A, adenine; C, cytosine; T, thymine; G, guanine; ds, double stranded; ss, single stranded; polI(k), *Escherichia coli* DNA polymerase I large (Klenow) fragment; εC, 3,$N^4$-ethenocytosine; εC·$H_2O$, hydrated 3,$N^4$-ethenocytosine [3,$N^4$-(hydroxyethano)cytosine]; εA, 1,$N^6$-ethenoadenine; εA·$H_2O$, hydrated 1,$N^6$-ethenoadenine [1,$N^6$-(hydroxyethano)adenine]; UV, ultraviolet.

0006-2960/90/0429-496$02.50/0 